Effects of Atomicity and Internal Polarization on the Electronic and Optical Properties of GaN/AlN Quantum Dots: Multimillion-Atom Coupled VFF MM-$sp^3d^5s^*$ Tight-Binding Simulations

Sasi Sundaresan, Krishna Yalavarthi, and Shaikh Ahmed, *Member, IEEE*

***Abstract*—Single-particle electronic structure and optical transition rates between the HOMO and LUMO states of a self-organized wurtzite GaN/AlN single quantum dot grown along the [0001] axis are calculated within an *atomistic 20-band* $sp^3d^5s^*$ tight-binding framework. The GaN/AlN quantum dot used in this computational study is realistically-sized (containing ~9 million atoms) and of truncated pyramid shape having height and base length of 4.5 nm and 23 nm, respectively. These reduced-dimensionality III-N structures are subject to competing effects of size-quantization and long-range internal fields that originate from: a) fundamental crystal atomicity and the interface discontinuity between two dissimilar materials; b) atomistically strained active region; c) strain-induced piezoelectricity; and d) spontaneous polarization (pyroelectricity). The *mechano-electrical* internal fields in the structure have been modeled using a combination of an *atomistic* valence force-field molecular mechanics (VFF MM) approach and a three-dimensional Poisson solver, and have found to strongly modulate the intrinsic single-particle electronic and optical properties of the quantum dots. In particular, in contrast to the well-studied InN/GaN systems, the effects of piezoelectric and pyroelectric fields *add up* (peak pyroelectric potential being *larger* than the piezoelectric counterpart) and result in a large redshift in the electronic bandgap near the Brillouin zone center (known as quantum confined stark effect), pronounced non-degeneracy in the excited states, strongly suppressed optical transition (increased recombination time), and anisotropic emission spectra.**

***Index Terms*—Quantum dot, nitride nanostructures, tight-binding, piezoelectricity, pyroelectricity, optical anisotropy.**

I. Introduction

RECENTLY, light emitters using *nanostructured* GaN/AlN active regions have attracted much attention due to several potential advantages, such as, wide range of emission frequencies (ultraviolet to red), high quantum efficiency, low noise, high color gamut, higher temperature stability of the threshold current and the luminescence, and low sensitivity to ionizing radiation [1]. The impacted markets include energy, digital information, healthcare and biotechnology, instrumentation, communications, and security.

Since the heteroepitaxy of GaN on AlN involves a lattice mismatch of ~2%, a form of Stranski-Krastanov mode can be used for growing GaN quantum dots (QDs) or disks on AlN by molecular beam epitaxy [2][3][4]. GaN QDs thus grown are strained in the AlN matrix and exhibit almost no inter-diffusion. The great majorities of GaN/AlN QDs crystallize in the thermodynamically stable wurtzite crystal structure and are grown along the polar [0001] direction. These structures generally exhibit spontaneous and strain-induced piezoelectric polarization, which lead to a large internal electrostatic field (on the order of MV/cm) and has a significant effect on the electronic and optical properties. In particular, it was demonstrated experimentally that the energy of the ground state optical transition in self-organized GaN/AlN QDs, depending on the size/thickness, may lie well below the *bulk* GaN band gap of ~3.44 eV [2].

Previous theoretical calculations of the electronic and optical properties of GaN/AlN QDs include multiband $\boldsymbol{k\bullet p}$ model [5] and tight-binding coupled with a continuum elasticity theory [6]. However, *continuum* representation (such as effective mass and $\boldsymbol{k\bullet p}$) suppresses the true fundamental atomistic symmetry of the underlying nanostructures thus *overestimates* the quantum yield of the light emitters in these QDs [7][8]. In our work, single-particle electronic structure and interband optical transition rates (between the HOMO and LUMO states) of self-organized wurtzite GaN/AlN single QDs with truncated pyramidal geometry and grown along the [0001] axis are calculated within an *atomistic* 20-band $sp^3d^5s^*$ tight-binding framework. On the other hand, long-range *mechano-electrical* internal fields in the structure have been modeled using a combination of an *atomistic* valence force-field molecular mechanics (VFFF MM) approach and a three-dimensional Poisson solver. Besides being more accurate in determining the bandgap, the *multiscale* approach employed here exposes the true atomistic symmetry of the structure that leads to unconventional non-degeneracy in the first excited state, band-mixing in the overall electronic states, and strongly suppressed and anisotropic inter-band transition rates.

II. Simulation Model

The overall simulation strategy is divided into four coupled phases: a) geometry construction; b) structural (strain) relaxation; c) computing the *long-range* internal fields; and d) determining the *atomistic* electronic structure and optical transitions. The purpose of the geometry constructor is to create (from a basis set) the nanostructure having wurtzite symmetry and store the atomistic details (type, coordinates, nearest neighbors, surface passivation, and computation type) in the memory of the computer. Ini-

Manuscript received June 12, 2012. This work is supported by National Science Foundation Grant No. 1102192.

The authors are with the Department of Electrical and Computer Engineering, Southern Illinois University at Carbondale, IL 62901 USA (phone: 618-453-7630; fax: 618-453-7972; email: ahmed@siu.edu).

tially, the atom positions in the entire computational domain (including those of GaN) are fixed to the AlN lattice constant. Then, the atom positions are relaxed and the resulting strain (mechanical) fields are calculated employing an atomistic valence force-field (VFF) method using the Keating potentials. In this approach, the total elastic energy of the sample is computed as a sum of bond-stretching and bond-bending contributions from each atom. The equilibrium atomic positions are found by minimizing the total elastic energy of the system. However, piezoelectricity is neglected in this step. The strain simulations fix the atom positions on the bottom plane to the AlN lattice constant, assume periodic boundary conditions in the lateral dimensions, and open boundary conditions on the top surface. The strain parameters used in this work are: $\alpha = 82.796$ for bond-stretching and $\beta = 15.098$ for bond-bending components, and are validated through the calculation of Poisson ratio of bulk materials. The small thermal strain contribution is neglected. Next, the calculation of the internal electrostatic fields is carried out. The overall polarization **P** in a typical wurtzite semiconductor is given by $\mathbf{P} = \mathbf{P}_{PZ} + \mathbf{P}_{SP}$, where $\mathbf{P}_{PZ}$ is the strain-induced piezoelectric polarization and $\mathbf{P}_{SP}$ is the spontaneous polarization (pyroelectricity). The piezoelectric polarization $\mathbf{P}_{PZ}$ is obtained from the diagonal and shear components of the anisotropic *atomistic* strain fields. In contrast, the spontaneous polarization is strain-independent and arises from fundamental asymmetry of the crystal structure. The polarization constants (in C/m^2) used in this study are as follows:

	ε_{15}	ε_{31}	ε_{33}	P_{SP}
GaN	0.326	-0.527	0.895	-0.034
AlN	-0.48	-0.58	1.55	-0.082

The polarization induced *charge density* is derived by taking divergence of the polarization. To do this, we divide the simulation domain into cells by rectangular meshes. The polarization of each *grid* is computed by taking an average of atomic polarization within each cell. A finite difference approach is then used to calculate the charge density by taking divergence of the grid polarization. Finally, the induced potential is determined by the solution of the 3-D Poisson equation on an atomistic grid (using an in-house PETSc-based parallel full 3-D Poisson solver). Next, the single-particle energies and wave functions are calculated using an empirical nearest-neighbor 20-band $sp^3d^5s^*$ tight-binding model. For this purpose we have augmented the open source NEMO 3-D tool and used the computational framework available therein. Detail description of this package can be found in Ref. [8][9]. Tight-binding is a local basis representation, which naturally deals with finite device sizes, alloy-disorder and hetero-interfaces. When needed, the piezoelectric and the pyroelectric fields are incorporated in the Hamiltonian as an external potential (within a semi-coupled approximation). Tight-binding results in very sparse matrices and the requirements of storage and processor communication are therefore minimal (compared to pseudopotential implementations [10]) and perform extremely well on inexpensive Linux clusters. The computational domain for the calculation of the electronic structure assumes a closed boundary condition with passivated dangling bonds. The tight binding parameters for GaN and AlN are taken from Ref. [11]. In the final phase, the *spontaneous* optical emission (absorption) rate is calculated by [12] using:

$$R\left(k_i,k_f,E\right)=\frac{2\pi}{\hbar}\frac{q^2A^2}{4m_0^{\,2}}\left|\vec{M}_{cv}\left(k_i,k_f\right)\cdot\hat{n}\right|^2\times \delta\left[E_v\left(k_f\right)-E_c\left(k_i\right)+E\right]\times F \quad (1)$$

where, $\vec{M}_{cv}$ is the momentum matrix calculated from the overlap of HOMO (valence) and LUMO (conduction) wavefunctions and F is the probability of hole occupation and electron vacancy, given by:

$$\vec{M}_{cv}\left(k_i,k_f\right)=\oint_{\Omega} d^3r\psi^*_{c,k_i}\left(r\right)\frac{\hbar}{j}\vec{\nabla}\psi_{v,k_f}\left(r\right), \quad (2)$$

$$F=f\left(E_v\left(k_f\right)-E_{fh}\right)\times\left[1-f\left(E_c\left(k_i\right)-E_{fe}\right)\right]. \quad (3)$$

For $F = 1$, emission (absorption) rate solely depends on the momentum matrix, where *absorption* and *emission* lose their meaning and we use a term *transition rate*. Note that for non-periodic finite-sized nanostructures (such as QDs), to calculate $\vec{M}_{cv}$, one needs to integrate in the entire domain. Since no free wave is available in a QD, $k_i = k_f = 0$ is the only available point used in the calculation.

III. Simulation Results

Figure 1 shows the simulated QD with truncated pyramid geometry. The GaN QD used in this study is grown in the [0001] direction and embedded in an AlN matrix and has base length, b~23 nm and height, h~4.5 nm, and are positioned on a GaN mono (wetting) layer. The simulation of strain is carried out in the large (rhombohedral) computational box (number of atoms ~9M), while the electronic structure computation is restricted to the smaller domain (number of atoms ~6M) with closed boundaries.

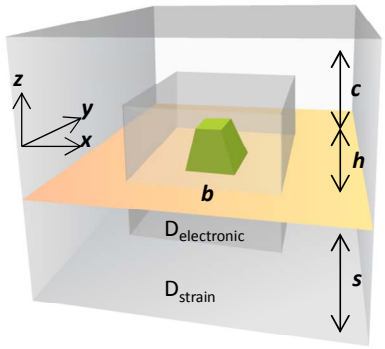

Figure 1. Simulated truncated pyramid GaN/AlN quantum dot on a thin (one atomic layer) GaN wetting layer. Two major computational domains are also shown. D_{elec}: central smaller domain for electronic structure (quantum) calculation, and D_{strain}: outer domain for strain calculation. Here, s is the substrate height ~30 nm, c is the cap layer thickness ~10 nm, h is the dot height ~4.5 nm, and d is the dot diameter ~23 nm.

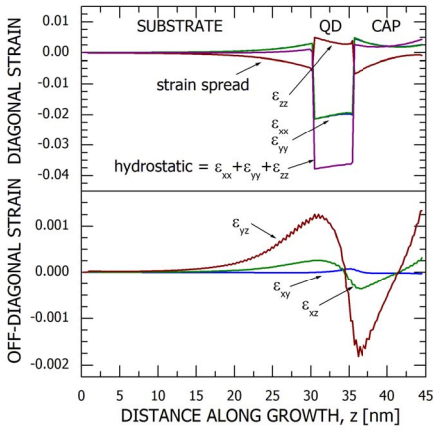

Figure 2. Atomistic strain along the growth ([0001]) direction through the center of the QD. Strain is seen to penetrate deep (more than 15 nm) into the substrate and the cap layers. Also, noticeable is the gradient of strain inside the dot region.

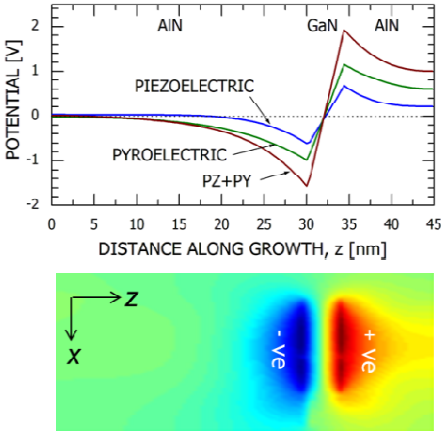

Figure 3. (top) Polarization induced potential along the [0001] direction. Note the large spread of the potential in the substrate and the cap layers. (bottom) Potential distribution (with lowered symmetry due to atomicity) in the XZ plane halfway through the width including both piezoelectric and pyroelectric contributions.

In the strain calculations, as shown in Figure 2, atomistic strain was found to be long-ranged (penetrating ~15 nm into the substrate and the cap layers) stressing the need for using realistically-extended structures (multimillion-atom modeling) in modeling electronic structure of these QDs. The overall hydrostatic strain ($\varepsilon_{xx}+\varepsilon_{yy}+\varepsilon_{zz}$) was found to be compressive within the QD and tensile in the AlN substrate and cap layers. Lower panel in Figure 2 shows the off-diagonal strain distributions in the [0001] direction through the center of the QD. The *inequivalence* of ε_{xz} and ε_{yz} components arise from the geometry of the system (truncated square pyramid in a rhombohedron).

The polarization-induced potential is calculated using a parallel full 3-D Poisson solver and shown in Figure 3. Both the piezoelectric and the pyroelectric potentials are found to be long-ranged, significantly large (peaks >1 eV), and anisotropic in the lateral and vertical planes (bottom panel). However, noticeable is the fact that the pyroelectric potential is larger and (in contrast to InN/GaN systems [9][13]) tends to *add up* with the piezoelectric counterpart.

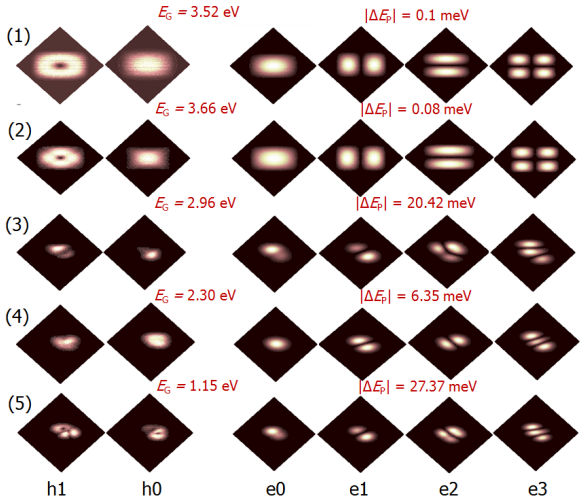

Figure 4. Two topmost valence and first four conduction band wavefunctions due to: 1) interface asymmetry, 2) strain relaxation, 3) piezoelectric, and 4) pyroelectric fields—all resulting in a shift in the energy bandgap. Wave functions in GaN dot showing deformed valence band, conduction band *P*-level anisotropy and non-degeneracy, and formation of mixed orbitals resulting from these competing fields

Next we calculate the *electronic structure* of the quantum dot. Here, we quantify the contributions of interface symmetry (without strain relaxation), strain, piezoelectricity, and pyroelectricity separately by calculating the bandgap (LUMO-HOMO), splitting in the conduction band *P* level, and wavefunction orientation. Figure 4 shows the two topmost valence and first four conduction band wavefunctions (projected on the X-Y plane). In the first row, where the effects of strain relaxation, piezoelectricity, and pyroelectricity are all excluded, the small split (non-degeneracy) in the *P* level (0.1 meV) is due mainly to the atomistic interface and fundamental material discontinuity in the underlying device structure. In the second row, atomistic strain relaxation is included resulting in a 0.08 meV split in the *P* level. In the third row, piezoelectricity is included on top of strain, which not only redshifts the bandgap by 0.7eV and induces a *P*-split of 20.42 meV but rotates the polarization in the *P* states and results in a mixed *D* band. In the fourth row, pyroelectric polarization is included on top of strain (without piezoelectricity). Pyroelectric polarization, while retaining the piezoelectric wavefunction orientation, has the strongest effect on the bandgap and results in a larger (1.36eV) redshift. In the fifth row, a combined effect of strain, piezoelectricity and spontaneous polarization is shown. The inclusion of all four internal fields results in mixed molecular orbitals, induces an overall *P*-split of 27.37 meV, and a bandgap of 1.15 eV! The large redshift of ~2.3 eV (as compared to experimental results on similar sized dots [2]) demands further careful investigation. Possible causes can be attributed to: a) use of a thicker QD in the simulation; b) use of *bulk* polarization constants (theoretically, polarization constants should depend on size-quantization); c) existence of non-linear second-order piezoelectric contribution that competes with and tends to cancel out the first-order counterpart (as seen in InAs/GaAs systems [10]); d) neutraliza-

tion of polarization charges in a real device/experiment due to surface/interface states and (dynamical) carrier screening; and e) interdiffusion causing a reduction in the gradient of polarization (charge density). Figure 5 summarizes the influence of the internal fields on the single-particle energy bandgap (left panel) and split in the *P* level (right panel).

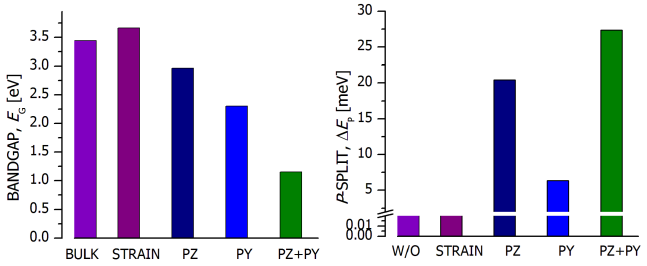

Figure 5. Bandgap (left) and split in *P* level (right) including interface effects (w/out strain), strain, piezoelectricity, and pyroelectricity.

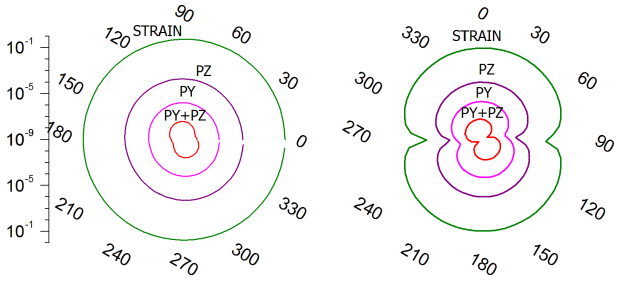

Figure 6. Interband optical transition rates projected on the XY (left) and the XZ (right) planes.

Figure 6 shows the polar plots of the interband optical transition rates between HOMO and LUMO in the QD projected on the XY plane (left panel) and the XZ (right panel) plane. The Figure reveals significant suppression (by several orders of magnitude) and strong polarization anisotropy in the optical emission due mainly to spatial irregularity in the wavefunctions. The true atomistic symmetry of the quantum dots, thus, influences the electronic bandstructure and reduces the transition rate by several orders of magnitude! The *in-plane* polarization degree (defined by $r = \frac{|I_{\max} - I_{\min}|}{|I_{\max} + I_{\min}|}$) for emissions in XY and XZ planes were found to be 0.58 and 0.96, respectively. The large reduction of optical transition rates and giant anisotropy in the emission characteristics (due mainly to wavefunction rotation in the XY plane and internal-field induced localization along the [0001] axis) suggest that improved design of light-emitters in these nitride systems would require QDs of smaller heights (disks) and better compositional matching.

IV. Conclusion

GaN/AlN nanostructures are excellent candidates for ultraviolet (UV) emitters. Electronic and optical properties of these reduced-dimensionality devices are strongly influenced by an intricate interplay of size-quantization and internal fields. Internal fields are long-ranged and atomistic in nature, which necessitate the need for using realistically-extended substrate and cap layers containing millions of atoms in the computational domain. Internal fields result in: a) deformed and localized wavefunctions; b) large red-shift in bandgap (quantum confined stark effect) as compared to the bulk value; c) pronounced degradation in transition rate; and d) reduced quantum efficiency and anisotropic emission spectra. In particular, pyroelectric/spontaneous polarization is very strong in GaN/AlN systems and the effects of piezoelectric and pyroelectric fields *add up*. Thinning down the dots (active region) is expected to improve the optical performance of these nanoscale light-emitters.

Acknowledgment

This work was supported by National Science Foundation Grant No. 1102192. Support for the computational resources from the ORAU/ORNL High-Performance Computing Grant 2009 is also acknowledged. The development of the NEMO 3-D tool involved a large number of individuals at JPL and Purdue University, whose work has been cited.

References

[1] M.S. Shur, R. Gaska, "Deep-Ultraviolet Light-Emitting Diodes," *IEEE Trans. Electron Devices*, vol. 57, 1, pp. 164–173, 2010.

[2] F. Widmann, J. Simon, B. Daudin, G. Feuillet, J. L. Rouvie`re, and N. T. Pelekanos, "Blue-light emission from GaN self-assembled quantum dots due to giant piezoelectric effect," *Phys. Rev. B*, vol. 58, 24, R15989, 1998.

[3] R. Bardoux, T. Guillet, B. Gil, P. Lefebvre, T. Bretagnon, T. Taliercio, S. Rousset, and F. Semond, "Polarized emission from GaN/AlN quantum dots: Single-dot spectroscopy and symmetry-based theory," *Phys. Rev. B*, vol. 77, 235315, 2008.

[4] J. Renard, R. Songmuang, C. Bougerol, B. Daudin, and B. Gayra, "Exciton and Biexciton Luminescence from Single GaN/AlN Quantum Dots in Nanowires," *Nano Lett*., vol. 8, 7, pp 2092–2096, 2008.

[5] A. D. Andreev and E. P. O'Reilly, "Optical transitions and radiative lifetime in GaNÕAlN self-organized quantum dots," *Appl. Phys. Lett*., vol. 79, 4, pp. 521–523, 2001.

[6] V. Ranjan,G. Allan, C. Priester, and C. Delerue, "Self-consistent calculations of the optical properties of GaN quantum dots," *Phys. Rev. B*, vol. 68, 115305, 2003.

[7] O. Marquardt, D. Mourad, S. Schulz, T. Hickel, G. Czycholl, and J. Neugebauer, "Comparison of atomistic and continuum theoretical approaches to determine electronic properties of GaN/AlN quantum dots," *Phys. Rev. B*, vol. 78, 235302, 2008.

[8] G. Klimeck, S. Ahmed, N. Kharche, H. Bae, S. Clark, B. Haley, S. Lee, M. Naumov, H. Ryu, F. Saied, M. Prada, M. Korkusinski, and T. Boykin, "Atomistic Simulation of Realistically Sized Nanodevices Using NEMO 3-D", *IEEE Trans. Electron Devices*, vol. 54, 9, pp. 2079–99, 2007.

[9] S. Ahmed, S. Islam, and S. Mohammed, "Electronic Structure of InN/GaN Quantum Dots: Multimillion Atom Tight-Binding Simulations", *IEEE Trans. Electron Devices*, vol. 57, 1, pp. 164–173, 2010.

[10] G. Bester, A. Zunger, X. Wu, and D. Vanderbilt, "Effects of linear and nonlinear piezoelectricity on the electronic properties of InAs/GaAs quantum dots", *Phys. Rev. B*, vol. 74, 081305, 2006.

[11] J. M. Jancu, F. Bassani, F. Della Sala, R. Scholz, "Transferable tight-binding parametrization for the group-III nitrides," *Appl. Phys. Lett*., vol. 81, 4838, 2002.

[12] E. F. Schubert, *Light-Emitting Diodes*, 2nd ed. University Press: Cambridge, 2008, pp 48–57.

[13] K. Yalavarthi, V. Gaddipati, and S. Ahmed, "Internal Fields in InN/GaN Quantum Dots: Geometry Dependence and Competing Effects on the Electronic Structure," *Physica E: Low-Dimensional Systems and Nanostructures*, vol. 43, pp. 1235–1239, 2011.